Pharm Res (2013) 30:2625–2639
DOI 10.1007/s11095-013-1088-2

RESEARCH PAPER

Development and Characterization of Nanostructured Mists with Potential for Actively Targeting Poorly Water-Soluble Compounds into the Lungs

Jerry Nesamony • Ashish Kalra • Mohamed S. Majrad • Sai Hanuman Sagar Boddu • Rose Jung • Frederick E. Williams • Alaina M. Schnapp • Surya M. Nauli • Andrea L. Kalinoski

Received: 26 February 2013 / Accepted: 19 May 2013 / Published online: 31 May 2013

ABSTRACT

Purpose To formulate nanoemulsions (NE) with potential for delivering poorly water-soluble drugs to the lungs.

Method A self nanoemulsifying composition consisting of cremophor RH 40, PEG 400 and labrafil M 2125 CS was selected after screening potential excipients. The solubility of carbamazepine, a poorly water-soluble drug, was tested in the formulation components. Oil-in-water (o/w) NEs were characterized using dynamic light scattering, electrophoretic light scattering, transmission electron microscopy (TEM) and differential scanning calorimetry. NEs were nebulized into a mist using a commercial nebulizer and characterized using laser diffraction and TEM. An aseptic method was developed for preparing sterile NEs. Biocompatibility of the formulation was evaluated on NIH3T3 cells using MTT assay. *In vitro* permeability of the formulation was tested in zebra fish eggs, HeLa cells, and porcine lung tissue.

Results NEs had neutrally charged droplets of less than 20 nm size. Nebulized NEs demonstrated an o/w nanostructure. The mist droplets were of size less than 5 μm. Sterility testing and cytotoxicity results validated that the NE was biocompatible and sterile. *In vitro* tests indicated oil nanodroplets penetrating intracellularly through biological membranes.

Conclusion The nanoemulsion mist has the potential for use as a pulmonary delivery system for poorly water-soluble drugs.

KEY WORDS cytotoxicity · *in vitro* permeability · nanoemulsions · poorly water soluble drug · pulmonary delivery system

ABBREVIATIONS

CBZ	carbamazepine
CLSM	confocal laser scanning microscope
DAPI	4′,6-diamidino-2-phenylindole
DLS	dynamic light scattering
DMEM	Dulbecco's Modified Eagle Medium
ELS	electrophoretic light scattering
FBS	fetal bovine serum
FTM	fluid thioglycollate medium
He-Ne laser	Helium-Neon laser
k_m ratio	surfactant/co-surfactant ratio
MH	Mueller Hinton
MTT	3-(4,5-dimethylthiazol-2-yl)-2,5-diphenyltetrazolium bromide
NE	nanoemulsions
OCT	optimal cutting temperature
PBS	phosphate buffered saline
SCD	soybean casein digest medium
SNE	self-nanoemulsifying
SNEDDS	self-nanoemulsifying drug delivery system

Electronic supplementary material The online version of this article (doi:10.1007/s11095-013-1088-2) contains supplementary material, which is available to authorized users.

J. Nesamony • A. Kalra • M. S. Majrad • S. H. S. Boddu • R. Jung
Department of Pharmacy Practice
College of Pharmacy and Pharmaceutical Sciences
University of Toledo, Toledo, Ohio, USA

F. E. Williams • A. M. Schnapp • S. M. Nauli
Department of Pharmacology
College of Pharmacy and Pharmaceutical Sciences
University of Toledo, Toledo, Ohio, USA

A. L. Kalinoski
Department of Surgery, College of Medicine and Biomedical Sciences
University of Toledo HSC, Toledo, Ohio, USA

J. Nesamony (✉)
Division of Industrial Pharmacy, Department of Pharmacy Practice
College of Pharmacy and Pharmaceutical Sciences, University of Toledo
HSC, 3000 Arlington Avenue, MS1013
Toledo, Ohio 43614, USA
e-mail: jerry.nesamony@utoledo.edu

INTRODUCTION

In recent years, there has been a growing interest in lipid-based formulations as a method for delivering poorly soluble drugs. One of the most promising technologies is self-nanoemulsifying drug delivery systems (SNEDDS). SNEDDS are isotropic mixtures of surfactant, cosurfactant, oil and drug that forms a fine O/W (oil-in-water) nanoemulsion (NE) when introduced into an aqueous medium under mild agitation (1). Nanoemulsion drug delivery systems are thermodynamically stable, transparent (or translucent) dispersions of oil and water stabilized by an interfacial film of surfactant molecules with a droplet size of less than 100 nm (2). When compared with emulsions, which are metastable dispersed forms, nanoemulsions are physically stable formulations (3). The nanosized droplets lead to large interfacial areas associated with NEs, which helps in sustained and targeted drug delivery by influencing the transport properties of the drug (4). The primary interest of formulating O/W nanoemulsions lies in their ability to enhance solubility of lipophilic drugs that are otherwise poorly water-soluble by incorporating them into the oil phase (2). Nanoemulsions have also been reported to increase the reproducibility of the plasma concentration profiles and bioavailability of hydrophobic drugs (5).

Carbamazepine (CBZ) is a lipophilic, poorly water-soluble compound that belongs to the class II drugs of the BCS (Biopharmaceutics Classification System) (6). CBZ is a widely used antiepileptic agent that has been effective in the therapy of psychomotor seizures and trigeminal neuralgia for 40 years. CBZ is usually administered orally as a solid, but due to its low solubility in water (about 170 mg/L at 24°C) its gastrointestinal absorption is slow and irregular (7). Incomplete bioavailaibility and considerable variability in its plasma concentration following oral administration have also been reported (8). Absorption of CBZ is primarily passive and is a function of lipophilicity (9), which makes it an ideal model drug for tissue permeability studies.

The pulmonary route is a noninvasive means to provide local lung effects and to enable systemic absorption. Avoidance of first-pass metabolism, enhanced patient adherence and the availability of a huge surface area for drug absorption are some of the major advantages of the pulmonary route over other drug delivery routes (10). In addition, metabolic activity in the lungs is relatively low (11).

In the presented research, we developed O/W nanoemulsions that were nebulized into novel nanostructured mists with the potential for pulmonary delivery. The nanoemulsions were evaluated for various physicochemical properties based on which a particular formulation was selected and optimized for drug delivery and loaded with CBZ. A sterilization technique was developed and validated according to United States Pharmacopeia (USP) method. Cell toxicity studies were performed in NIH3T3 cell cultures for the sterile formulation to determine biocompatibility. Finally, the nanoemulsion was loaded with a water-insoluble but oil-soluble fluorescent dye, and diffusion characteristics were evaluated in zebra fish eggs, HeLa cell cultures, and porcine lung tissue.

MATERIALS AND METHODS

Materials

Labrasol®, Capryol™ 90, Transcutol® P, Labrafil M 2125® CS (LM 2125 CS), and Labrafac Lipophile WL 1349 (LL WL 1349) were provided by Gattefosse, St. Priest, France. Cremophor® RH 40 was supplied by BASF Chemicals,USA. Isopropyl myristate (IPM), Tween 80 and Polyethylene Glycol 400 NF (PEG 400) were purchased from Spectrum Chemicals. Carbamazepine was purchased from PCCA. Sudan IV, methanol (HPLC grade) and acetonitrile (HPLC grade) were obtained from Fisher Scientific. All other chemicals were of analytical grade.

Methods

Solubility Studies of Carbamazepine

CBZ was selected as a model drug to investigate the utility of the nanoemulsions to incorporate poorly water-soluble compounds. The solubility of carbamazepine in various excipients used in trial formulations was determined from a calibration curve of carbamazepine in methanol, using reverse phase HPLC (Waters e2695 separation module). An excess amount (~500 mg) of carbamazepine was added to 4 ml of each excipient in a microcentrifuge tube and vortexed for 5 min. Drug-excipient mixtures were equilibrated at 40°C in a water bath to facilitate solubilization. The mixture was finally placed at ambient room temperature (25°C) under continuous shaking for 48 h (12). The mixtures were then centrifuged at 3,000 rpm for 20 min. Aliquots of supernatants were prepared and diluted using methanol, and the drug content was quantitatively determined *via* HPLC using a C_{18} reverse phase column (Symmetry C_{18} column - 3.5 μm, 4.6×75 mm) and a mobile phase comprised of water/methanol/acetonitrile (60/20/20) at a flow rate of 1.0 ml/min. The absorbance measurement was performed at 285 nm using PDA detector connected to the HPLC separation module and data analysis performed in the Empower software.

Evaluation of Self-Nanoemulsifying Property and Ternary Phase Diagrams

The unique property of self-nanoemulsification is exhibited by only certain surfactants, co-surfactants, and oil combinations

in specific compositions. Cremophor RH 40, Tween 80 and Labrasol were used as surfactants. PEG 400, Transcutol P and Capryol 90 were used as cosurfactants. Labrafil M 2125 CS (LM 2125 CS) was the selected oil in the trial formulations. A total of nine self-nanoemulsifying (SNE) mixtures were prepared containing a particular surfactant, co-surfactant, and oil in various proportions. The oil:(surfactant/cosurfactant) ratios tested included 1:1, 1:2, 1:3, 1:4, 1:5, 1:6 and 1:7. The surfactant/cosurfactant ratio, also known as the k_m ratio, was evaluated by changing the proportions as 1:1, 2:1 and 3:1. Thus, nine surfactant-cosurfactant-oil combinations, totaling 21 different compositions, were evaluated for their self-emulsifying properties.

A test for self-emulsification was conducted on all nine SNE mixtures according to a method reported by Craig *et al.* (13). 0.6 ml of each SNE mixture was added to 400 ml of DI water under gentle agitation using a magnetic stirrer. The emulsification time, clarity of the emulsion, and apparent stability were visually evaluated and documented. The combinations that produced a clear and transparent nanoemulsion with no signs of instability for 24 h were plotted on a ternary phase diagram using SigmaPlot® software version 12.0. After examining the phase diagrams, an optimal formulation was selected for further development and characterization.

Drug-Loaded Nanoemulsions

The SNE mixture consisting of Cremophor RH 40 (50%): PEG 400 (25%): Labrafil M 2125 CS (25%) was selected for drug loading based on evaluation of the nanoemulsifying properties of the SNE mixtures. 100 mg of CBZ was added to 5 g of the SNE mixture and vortexed until it was completely solubilized. A nanoemulsion was prepared from the SNE mixture by gently mixing an aliquot of the mixture in 400 ml DI water as described earlier.

Droplet Size Analysis of Nanoemulsions

The droplet size of the NE (with and without drug) was determined by dynamic light scattering instrument (DLS) (Nicomp 380 ZLS). Volume weighted diameter was measured by placing samples taken in disposable Durex® borosilicate glass culture tubes in a sample chamber maintained at 23°C placed in the path of a He-Ne laser (λ of 658 nm). The scattered light was collected at an angle of 90° and detected by an avalanche photodiode array detector. The data analysis was performed by the accompanying software and expressed as a volume-weighted diameter. The measurements were done in triplicate. The droplet size was also determined after filtering the nanoemulsion through a 0.2 μm Nalgene® syringe filter (25 mm surfactant free cellulose acetate membrane) attached to a syringe.

Zeta Potential Analysis of Nanoemulsions

The zeta potential analysis was performed in the DLS instrument operating in the electrophoretic light scattering mode (ELS) (Nicomp 380 ZLS, Particle Sizing Systems, CA). Samples were taken in standard 1 cm square glass cuvettes and placed in a thermostated sample chamber maintained at 23°C. The electrode assembly fit into the cuvette, and readings were made by collecting the scattered laser light at an angle of 14.1°C. The zeta potential for each trial formulation was measured in triplicate.

Differential Scanning Calorimetry

Thermal behavior of the formulation and physical state of the incorporated CBZ were determined using a differential scanning calorimeter (Diamond DSC, PerkinElmer) equipped with an intercooler 1P. Samples weighing approximately 3 to 5 mg of SME mixture, both with and without drug, were placed in standard 20 μl aluminum pans. The samples were exposed to a thermal program that increased the temperature from 23°C to 250°C at the rate of 10°C/min. The data was analyzed using Pyris Manager 1.3 software.

Transmission Electron Microscopy

Transmission electron microscopy (TEM) was used to study the morphology of the O/W NE droplets. A Hitachi HD-2300 scanning transmission electron microscope was used in transmission electron mode to collect individual droplet images. A drop of the NE was placed on a holey carbon 400 mesh copper grid (Ted Pella®, CA) and equilibrated at room temperature for 24 h by placing in a closed chamber before obtaining electron micrographs. The images were captured and optimized using Quartz PCI software version 8.

Size and Morphology of Nanostructured Mists

Nanoemulsions with and without CBZ were nebulized to examine their potential for pulmonary delivery. The O/W NE was nebulized by placing 3 ml NE in a pediatric micromist jet-type nebulizer attached to a piston compressor. The mist was generated in the sample chamber of a particle size analyzer (Microtrac Aerotrac SPR 7340) equipped with a 1 mW He-Ne laser (λ of 632.8 nm). The data collected were analyzed using proprietary LDSA Win 6.21 software available with the instrument.

In addition, the morphology of the nanoemulsion droplets in the nebulized mist was studied using a TEM. A holey carbon 400 mesh copper grid (Ted Pella, Inc.) was positioned in the adapter of the pediatric nebulizer, channeling the stream of nanoemulsion mist as it was ensuing out of the nebulizer for approximately 60 s with the help of a self-

locking tweezer. The grid was then equilibrated at room temperature for 24 h before it was finally analyzed under the electron microscope.

Development and Validation of Sterilization by Filtration

All trial nanoemulsion formulations were sterilized *via* a filtration method. Validation of the sterilization method was performed using direct and plate inoculation according to USP recommendations (14). Fluid thioglycollate medium (FTM) and soybean casein digest medium (SCD) were used for direct (tube) inoculation method. All tests were carried out under aseptic conditions in a laminar airflow hood.

Identical test tubes were prepared for FTM and SCD media as follows. For direct inoculation, there were negative control tubes, positive control tubes, positive sample control tubes and aseptically filtered nanoemulsion sample tubes. The negative control contained 9 ml of the uninoculated medium and 1 ml of sterile water. The positive controls were prepared using *Staphylococcus aureus* ATCC 25923 cultured on an MH agar plate and incubated at 35°C for 24 h. Bacterial colonies on the plate were swabbed and placed into a test tube containing 5 ml of sterile water and another containing 5 ml of nanoemulsion. The bacterial concentration was determined using a Spectronic 20 Genesys Spectrophotometer (Spectronic Instruments) at 625 nm. Sterile water was used as a blank, and the sample absorbance was compared to a 0.5 McFarland Standard (1.5 CFU/ml). Serial dilutions of the standard were performed to achieve final concentrations of 10^2 CFU/ml. Positive controls contained 9 ml of medium and 1 ml of water containing 10^2 CFU/ml. Positive sample controls contained 9 ml of medium and 1 ml of nanoemulsion containing 10^2 CFU/ml. The aseptically filtered NE sample test tubes contained 9 ml of the medium and 1 ml of the NE that was aseptically passed through a 0.2 μm Nalgene® syringe filter attached to a syringe. The FTM tubes were incubated at 35°C. One set of SCD tubes was incubated at 35°C and another set of SCD tubes was incubated at room temperature (approximately 20°C) (15).

Samples of 400 μl were withdrawn from each of the test tubes from direct inoculation method on days 0, 7 and 14. These samples were transferred into microcentrifuge tubes and then spiroplated onto Mueller Hinton (MH) agar plates using SpiralBiotech Autoplate 4000 instrument. The machine stylus underwent a wash cycle using bleach, followed by two wash cycles using water, after each plating was completed (15).

In Vitro Cytotoxicity Test

In vitro cytotoxicity of the formulation (without drug) was tested on NIH 3 T3 cell line ATCC CRL-1658 (mouse embryonic fibroblasts). Cells were subcultured in Dulbecco's Modified Eagle Medium (DMEM) containing 5% fetal bovine serum and penicillin/streptomycin. Cells were then transferred to a 96-well plate and incubated at 37°C in 5% CO_2 environment for 24 h. After incubation, the medium in the wells was replaced with fresh DMEM media. The 96-well plates consisted of 4 wells of negative control containing only DMEM medium, 4 wells of positive control containing cells in DMEM medium, and 4 sample wells each containing nanoemulsion in DMEM medium in concentrations of 11%, 5.5%, 0.5%, 0.25% and 0.125% respectively. After 48 h of incubation, 10 μl of MTT reagent was added to all the wells and carefully mixed, and the plate was incubated for another 4 h. The 96-well plate was checked for absorbance using BioRad absorbance plate reader with the wavelength set at 580 nm. The MTT assay data was statistically analyzed using single factor analysis of variance (ANOVA) test.

In Vitro Permeability Tests

Three *in vitro* permeability tests were performed to analyze the location of the nanoemulsion in biological systems including porcine lung tissue, zebra fish eggs, and HeLa cell cultures. Sudan IV was used as a fluorescent marker to aid in detection of the nanoemulsion *via* confocal laser scanning fluorescence microscopy. Sudan IV is an oil-soluble azo dye that is practically insoluble in water (16). It is a marker that preferentially partitions into lipophilic domains and hence is used as a stain while imaging through optical microscopy and immunohistochemistry (17). The SNE mixture containing Cremophor RH 40, PEG 400, and Labrafil M 2125 CS was loaded with Sudan IV. The solubility of Sudan IV in the excipients was determined by UV–vis spectrophotometry (Agilent UV spectrophotometer 8453)(18). A procedure identical to the one used to determine CBZ solubility in excipients was used. The sample absorbances were measured at 522 nm. 50 mg of the dye was solubilized in 1 g of Labrafil M 2125 CS, and the nanoemulsion was prepared as previously described except that dye-containing oil was used in the SNE mixture instead of blank oil. Droplet size distribution and zeta potential measurements were also performed on dye-loaded NEs to analyze the impact of the entrapped dye on the NE characteristics.

In Vitro Permeability Studies in Zebra Fish Eggs

Zebra fish (*Danio rerio*) is currently a widely used model used to study development and toxicology. Females can produce up to 300 externally fertilized embryos in a week and initial development is completely transparent. The choice of zebra fish eggs to study formulation permeability in this work was due their excellent suitability to perform imaging *via* microscopy. From fertilization to up to 24 h post fertilization, the embryos are remarkably transparent with no color, and have extremely low autofluorescence.

The research involving zebra fish eggs adhered to the "Principles of Laboratory Animal Care" (NIH publication #85-23, revised in 1985). Adult zebrafish were purchased from the Zebrafish International Resource Center (ZIRC) at the University of Oregon (Eugene, OR; P40 RR012546 from NIH-NCRR). The fish were kept in fish tanks containing buffered water (pH 7.2) at 28°C and were fed daily live brine shrimp naupli and Tetramin dried flake food (Tetra, Blacksburg, VA). The day:night cycle was maintained at 14 h:10 h, and spawning and fertilization were stimulated by the onset of first light. Marbles were used to cover the bottom of the spawning tank to protect newly laid eggs and facilitate their retrieval for study. Fertilized zebrafish embryos were collected from the bottom of the tank by siphoning with a disposable pipette. The eggs were placed in Petri dishes and washed thoroughly with buffered egg water (deionized water containing 60 mg sea salt (Instant Ocean, Mentor, OH) per liter of water). Groups of 10 fertilized eggs were then placed in individual wells of 6-well plates, each well containing 3 ml of buffered egg water and used in the experiments. The exposure study comprised of negative control, positive control, and dye-NE wells. The eggs were exposed to only egg water in the negative control. In the positive control the eggs were exposed to 500 µl of blank NE devoid of the dye. In the dye-NE well, one set of eggs was exposed to 500 µl of NE containing 50 mg/mL of Sudan IV, and another was set exposed to 500 µl of NE containing 100 mg/mL of Sudan IV. After 6 h of exposure, the eggs were washed thoroughly with buffered egg water and were visualized in a Leica TCS SP5 multiphoton confocal laser scanning microscope (CLSM). The excitation beam splitter was set to 488/561 nm, and the emission bandwidth was set to 501 nm to 571 nm.

In Vitro Permeability Studies in HeLa Cells

HeLa cells were grown as a monolayer culture in DMEM supplemented with 10% fetal bovine serum (FBS), 2 mmol/1 L-glutamine and penicillin/streptomycin (100 units/ml), at 37 C in 5% CO2 humidified atmosphere and passaged when 70–80% confluent. Cells in exponential growth phase were trypsinized (0.05% trypsin-0.02% EDTA solution) and seeded at 50,000 cells per well in 6 well-plates containing a circular glass cover slide and complete media. Cells were allowed to adhere for 72 h and media replaced by the appropriate experimental and control formulations for 2 h. Experiments were performed in duplicate with negative control wells containing plain media, positive control wells containing blank NE, and NE formulation containing 100 microgram dye/ml of the formulation. After exposure, the formulations were removed and each well washed with 1 ml of phosphate buffered saline (PBS) three times and 1 ml of complete media was added to each well. The cover slides were removed using clean and sterile tweezers, appropriately mounted and visualized in a Leica TCS SP5 confocal laser scanning microscope (CLSM). Samples were excited with a 488 argon laser and emission collected in the 499 to 584 nm range.

In Vitro Permeability Studies in Porcine Lungs

Porcine lung from a freshly sacrificed pig was obtained from a local slaughterhouse. The lungs were sectioned along a coronal plane. The tissue sections used in the permeability experiments consisted of circular pieces of 1 cm diameter and 1 cm thickness. The washed lung sections were placed between the donor and receptor chamber of 15 ml Franz diffusion cells and equilibrated for 45 min at 40°C in a water bath. The lung sections were placed to simulate the actual physiological state in which the inner side of the lung was facing the donor chamber where the formulations were placed. The permeability study set up comprised of a negative control, a positive control, and dye-NE (100 mg Sudan IV/mL of the formulation) cells. To the negative control cells, 2 ml of phosphate buffered saline (PBS – pH 7.4) was added to the donor chamber. 2 ml of blank nanoemulsion devoid of Sudan IV was added to the positive control cell. Dye-NE cells contained 2 ml of the dye containing nanoemulsion. After an hour, the tissue was removed from the assembly and frozen at −80°C. A section of the frozen tissue was mounted on a metal chuck using optimal cutting temperature (OCT) compound. A cryostat fitted with a rotary microtome was used to cut 30 µm thick sections of the tissue. The sections were mounted on a glass slide, and a drop of DAPI was added to counter-stain the tissue (19). The slides were dried for 24 h and then were observed under a 10X objective in a Nikon TiU microscope coupled with photometric Coolsnap EZ 20 MHz camera (Photometrics, Tuczon, AZ). All images were acquired and processed using the Metamorph software (version 7.6.5.0). An excitation wavelength of 325 to 375 nm and a blue filter were used when DAPI stain was visualized. When Sudan IV was analyzed, an excitation wavelength of 460 to 500 nm and a FITC filter were chosen to process the image.

RESULTS AND DISCUSSION

Solubility Studies of Carbamazepine

In an O/W microemulsion, the solubility of the drug in the oil governs the drug carrying capacity of the microemulsion system. Since the formulation reported in this manuscript was being developed as a delivery system for poorly water-soluble compounds, CBZ which is slightly soluble in water, was expected to demonstrate good solubility in the materials that were screened for trial formulations. Table I lists the

Table I Solubility of Carbamazepine in Various Excipients

Type of excipient	Excipient	Solubility (mg/ml)
Surfactant	Cremophor RH 40	26.25 ± 0.53
	Labrasol	143.2 ± 3.8
	Tween 80	85.5 ± 1.77
Cosurfactant	PEG 400	291.75 ± 13.61
	Capryol 90	101.975 ± 2.67
	Transcutol p	151 ± 5.9
Oil	Labrafac PG	10.05 ± 1.02
	Labrafil M 2125 CS	38.125 ± 0.92
	Labrafac Lipophile WL 1349	7.525 ± 0.97
	Isopropyl myristate	6.375 ± 0.62
Solvent	Methanol	211.75 ± 10.43
	Water	0.15 ± 0.07 (Practically insoluble)

solubility of CBZ in various excipients tested. CBZ exhibited maximum solubility in Labrafil M 2125 CS among the various oils tested. The solubility of CBZ in the tested oils was dependent on the polarity of the oils. The polarity of the oils increased according to the order LL WL1349 < Labrafac PG < LM 2125 CS < IPM. CBZ solubility in the oil of highest polarity and in the oil of lowest polarity value was in similar range. However, in oils of intermediate polarity, the solubility was higher than in extremes. It appears that an optimal polarity range facilitates CBZ solubility (20). The generalization applicable in surfactants is as follows. The HLB of all the surfactants was similar, but CBZ solubility was found to increase in the following order: Tween 80 < Cremophor RH 40 < Labrasol. A possible explanation for this is that the branching in the alkyl chains increases in the same order as the solubility, potentially enabling accommodation of the poorly water-soluble CBZ when voids are created by molecular mobility within the surfactant. Similar effects were observed when studying solubility of poorly water-soluble substrates in surfactants by other researchers (21). When comparing CBZ solubility between various co-surfactants, it is evident that in addition to polarity and steric effects, H-bonding may modulate solubility of the model drug in various solvents as well. An ongoing study in our research group involves evaluation of lipid solubility and stability of poorly water-soluble compounds in lipid-API mixtures.

Evaluation of Self-Nanoemulsifying Property and Ternary Phase Diagrams

The evaluation of the self-nanoemulsification property of the excipients helped to determine specific combinations of excipients and their relative amounts needed to prepare a trial nanoemulsion formulation. The test of emulsification demonstrated that only six of the nine combinations tested exhibited

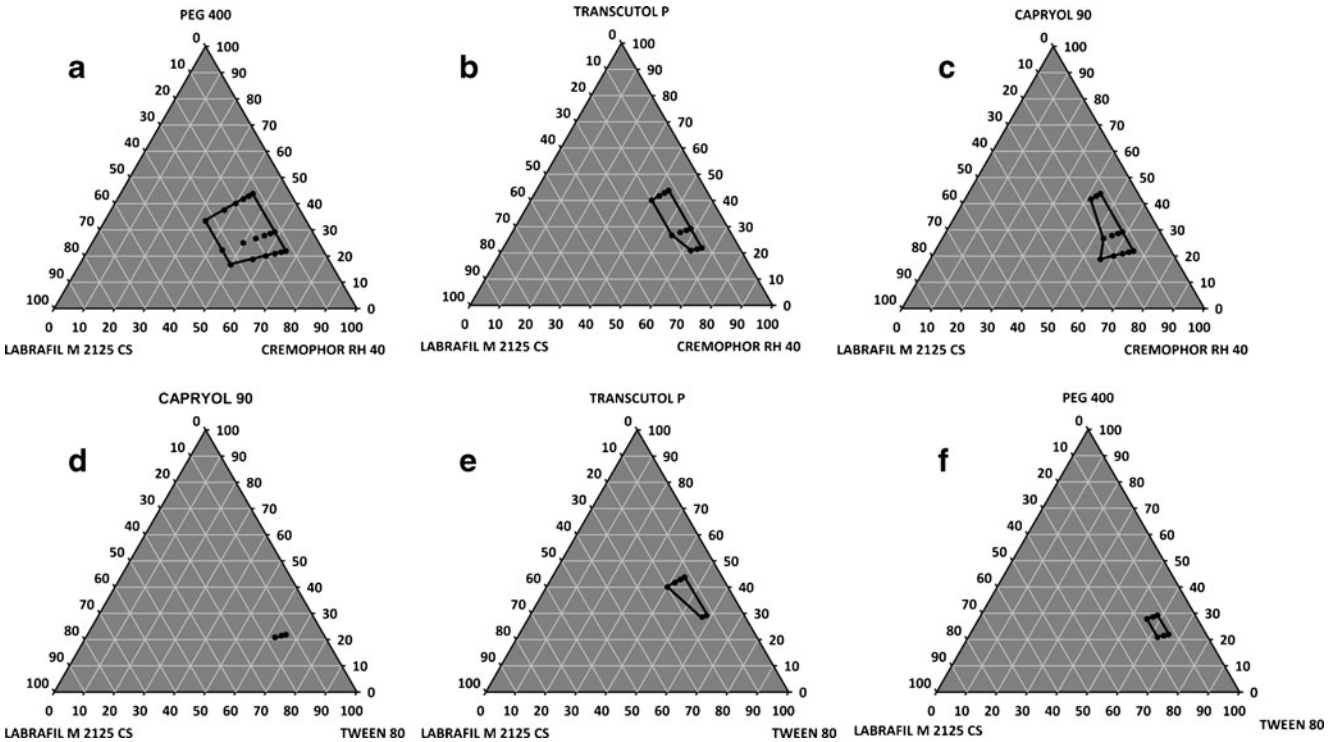

Fig. 1 Ternary phase diagrams of combination (**a**) Cremophor RH 40 : PEG 400 : Labrafil M 2125 CS (**b**) Cremophor RH 40 : Transcutol P : Labrafil M 2125 CS and (**c**) Cremophor RH 40 : Capyrol 90 : Labrafil M 2125 CS (**d**) Tween 80 : Capyrol 90 : Labrafil M 2125 CS (**e**) Tween 80 : Transcutol P : Labrafil M 2125 CS and (**f**) Tween 80 : PEG 400 : Labrafil M 2125 CS.

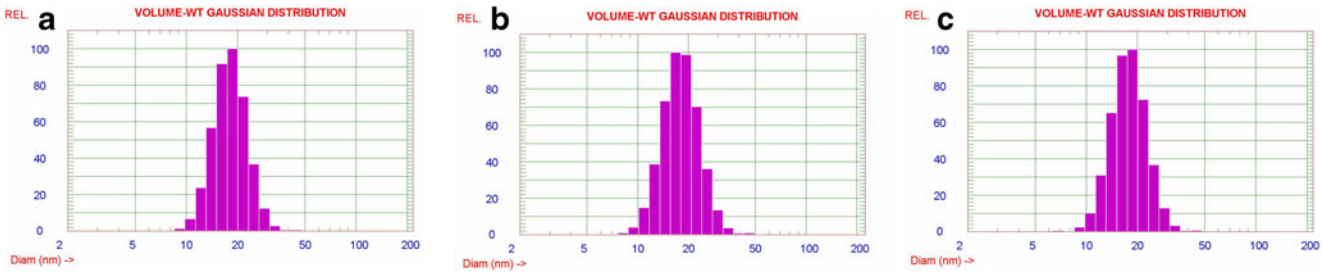

Fig. 2 (**a**) Droplet size distribution of blank nanoemulsion (**b**) Droplet size distribution of CBZ loaded nanoemulsion (**c**) Droplet size distribution of blank nanoemulsion after filtration.

this property. The time required by SNE mixtures to disperse into a clear and transparent NE that was stable for a period of 24 h was also noted. The stable combinations were plotted on ternary phase diagrams to determine the emulsification area. The SNE mixture with the largest emulsification area was considered a better SNE mixture when compared to the other combinations since this mixture was capable of producing a NE over a wide range of compositions (2). Figure 1a–f shows ternary phase diagrams of the six SNE mixtures evaluated for emulsification. It is evident that SNE mixtures containing Cremophor RH 40 possess the largest nanoemulsion regions in the phase diagram. Among these three SNE mixtures, Cremophor RH 40: PEG 400: Labrafil M 2125 CS mixtures emulsified in the least time. The tendency to form a stable nanoemulsion was observed to be highly dependent on the nature of the components and the composition. Cremaphor RH 40 produced stable NEs over a range of concentrations and combinations with the oil and co-surfactants screened, and hence it was selected as the surfactant for future formulations. Similarly PEG 400 was chosen as the co-surfactant since it enabled preparation of a greater number of trial formulations in combination with the other ingredients. This is an important criterion to be considered at this stage. Since the overall goal is to develop a drug delivery system, compositions that offer greater flexibility with regard to excipient concentrations may accommodate active ingredients with a range of solubilities during the drug loading phase of the study. An additional consideration that was taken into account when deciding the final composition of the SNE mixture was the nanoemulsification time. The SNEs that produced stable NEs self-nanoemulsified over a range of times, with the lowest emulsification time noted as 20 s and the highest time required at over 300 s. Based on their ability to form SNEDDS, Cremophor RH 40 and PEG 400 were selected as the surfactant and cosurfactant, respectively, since they formed the most stable nanoemulsion in the shortest time in combination with Labrafil M 2125 CS. The concentration of excipients present in the trial formulations was well within the range tolerated in biological systems (22,23). Nanoemulsions form spontaneously or under gentle mixing when the HLB of the surfactant used in the preparation is well balanced. Alternatively, surfactants that are highly oil-soluble or highly water-soluble are unable to stabilize the monolayer around the oil nanodroplet when the components are mixed. Proposed theories on spontaneity of nanoemulsion formation and its thermodynamic stability expound on the polarity of the surfactant, presence of ultralow interfacial tension, and orientation of molecules at the oil–water interface as conditions necessary for formation of NEs .

Drug Loading of SNEDDS

Based on emulsification time, ternary phase diagrams and drug solubility studies, a SNE mixture comprised of Cremophor RH 40 (50% w/w) : PEG 400 (25% w/w) :

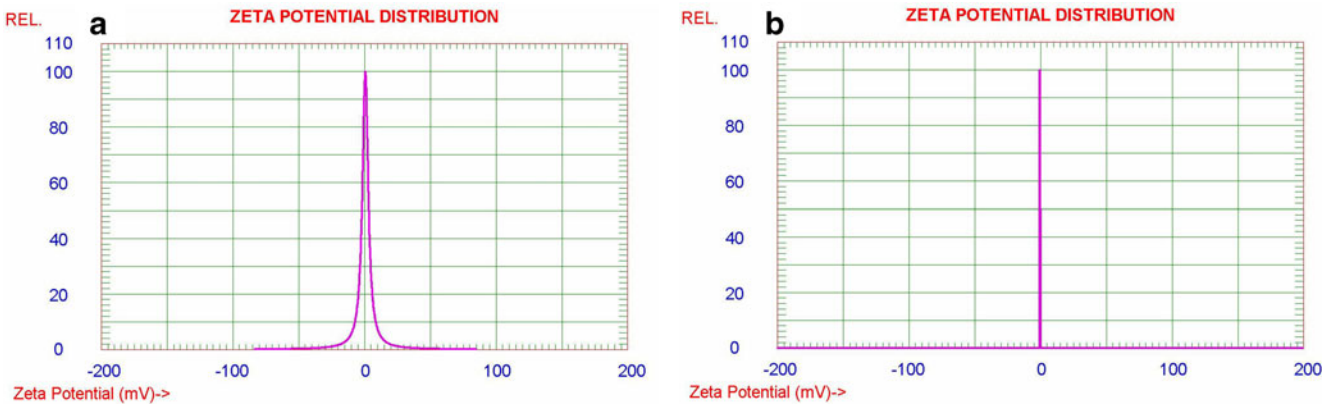

Fig. 3 Zeta potential of (**a**) blank microemulsion and (**b**) CBZ containing microemulsion.

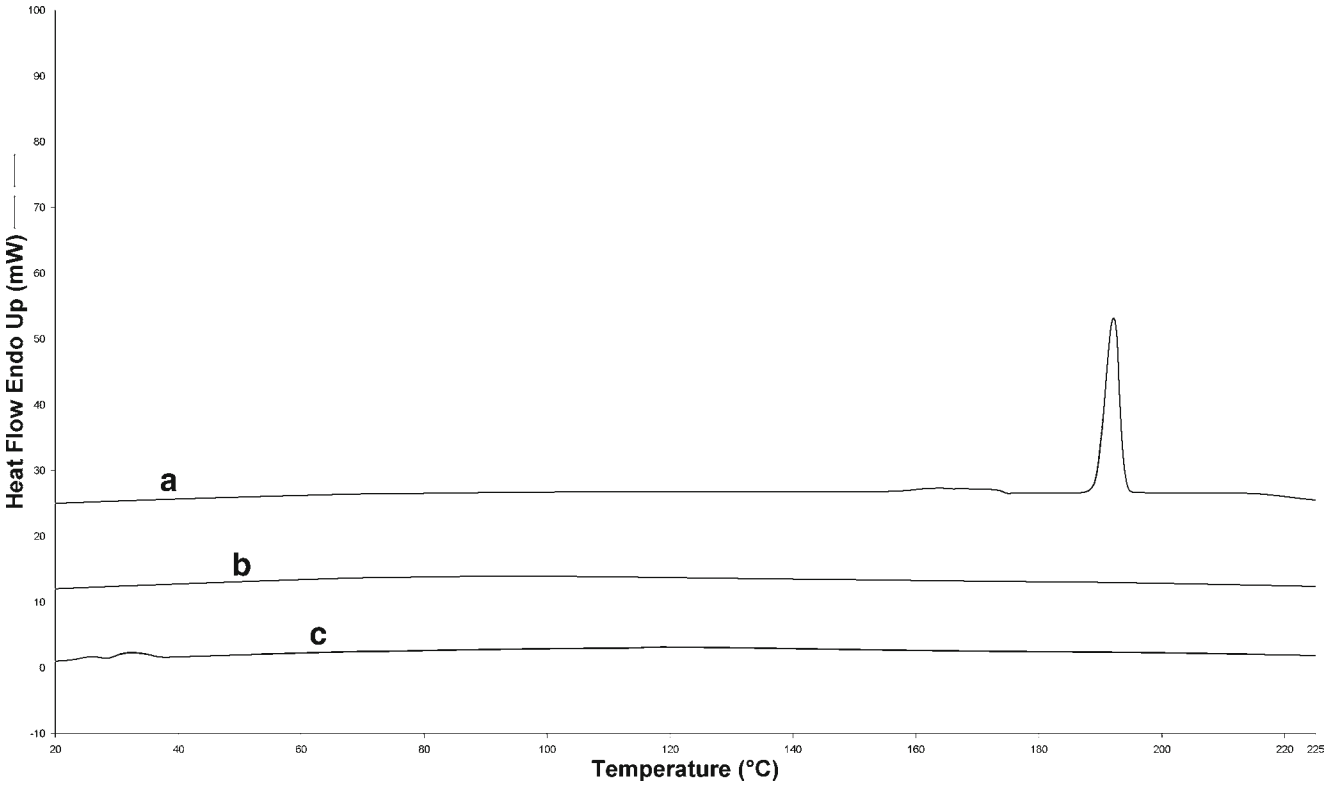

Fig. 4 DSC thermogram of (**a**) Carbamazepine (**b**) blank nanoemulsion and (**c**) Carbamazepine loaded nanoemulsion.

Labrafil M 2125 CS (25% w/w) was chosen for incorporating the model drug, CBZ. The solubility of CBZ in the SNE mixture as determined by HPLC was found to be 376.6± 0.61 mg/ml. The drug dissolved in the selected SNE mixture and exhibited no visual indication of phase separation and precipitation over a period of 1 month. CBZ containing SNE mixture was subjected to the test of emulsification as described in the "Materials and Methods" section. The samples displayed identical patterns of emulsification when compared to the data obtained from blank formulations. The CBZ-SNE mixture formed a visually clear and transparent nanoemulsion when mixed with water. The pH of the blank NE was found to be 5.8±0.1 and that of CBZ loaded NE was 5.9±0.1. The nanoemulsions also did not show any signs of drug precipitation, discoloration, or phase separation when observed over a period of 1 month. The effect of pH, ionic strength and constituents such as polymers on the phase behavior of micro- and nanoemulsions is generally related to the nature of the surfactants used in the formulation. The microstructure and dynamics of preparations containing ionic surfactants have been affected more than systems comprising of non-ionic surfactants (24,25). Formulations containing components similar to the ones reported in this work were found to accommodate a variety of drugs and pharmaceuticals with no significant effect on the physico-chemical properties of the formulation (12,26).

Droplet Size Analysis of Nanoemulsions

The droplet size of blank and drug-loaded nanoemulsion was found to be 18.5±0.6 nm (Fig. 2a) and 18.6±0.3 nm (Fig. 2b), respectively. The presence of CBZ did not significantly modify the droplet size and size distribution of the formulation. When the formulation was filtered through a

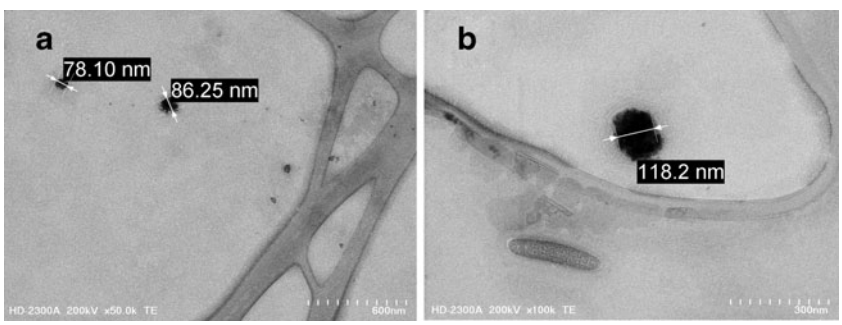

Fig. 5 Representative TEM images of (**a**) blank SNEDDS (**b**) CBZ loaded SNEDDS.

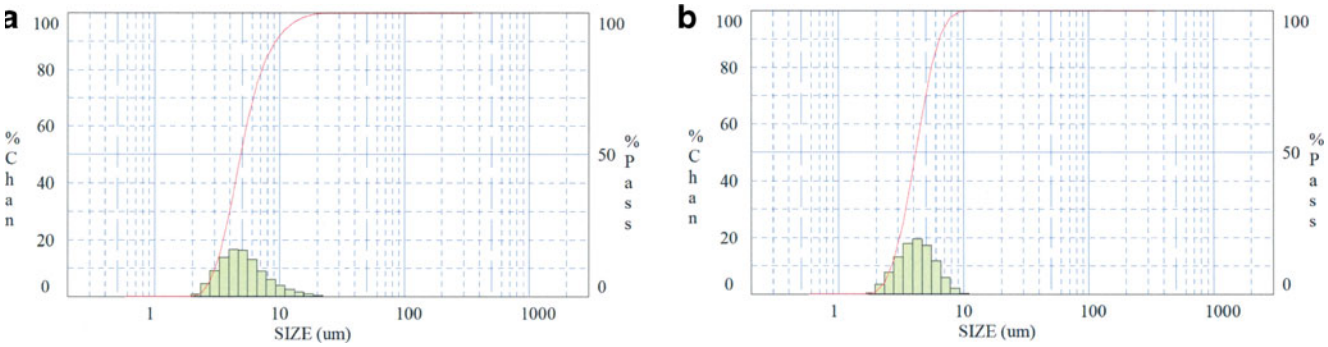

Fig. 6 Particle size distribution of (**a**) blank nanoemulsion mist and (**b**) CBZ loaded nanoemulsion mist.

0.2 µm filter, the droplet size remained unaltered at 18.3 ± 0.7 nm (Fig. 2c), indicating that the nanoemulsion is capable of retaining its original shape and size upon filtration. This finding was significant, given the objective of this work to develop a formulation that can be administered *via* inhalation. Steam sterilization, the most common method of sterilization, was ruled out as a method to make the formulations aseptic due to concerns about thermal stability of the oil in the presence of the moisture and heat. In addition, the temperature-dependent solubility of the surfactant could compromise the physical stability of NEs when autoclaved. In addition to providing a lipid core to solubilize poorly water-soluble drugs, the NE oil droplets that are less than 100 nm in diameter play a vital role in increasing the rate and extent of drug absorption (27). Small oil droplets can facilitate rapid breakdown of the triglycerides carrying the drug, leading to rapid drug release (28). The small particle size of the reported formulations further makes it acceptable for delivery *via* various routes, including transdermal, pulmonary, nasal, and parenteral administration (29,30).

Zeta Potential Analysis of Nanoemulsions

The zeta potential for blank and drug-loaded nanoemulsions was observed to be neutral (Fig. 3). Formulations such as micro- and nanoemulsions increase the bioavailability of poorly water-soluble compounds through multiple mechanisms including improved drug dissolution, increased membrane permeability *via* enhanced biomembrane fluidity, increased tight junction permeability, and inhibition of p-glycoprotein efflux pumps (31). The latter three mechanisms are dependent on the surface properties and surface charge of the oil droplets. Ionic surfactants and anionic and cationic components that are amphiphilic have been used to impart both positive and negative surface charge on oil nanodroplets. There are purported advantages associated with a positive or negative surface charge. A positively charged surface strongly interacts with the negative biological interfaces but leads to high cytotoxicity. A strong interaction between the nano droplets and biological membranes is associated with augmented cellular permeability of the incorporated drug. A negative surface charge produces weak interactions with biological membranes causing smaller gains in cellular permeability (28). Consequentially negative charged systems are better tolerated in biological systems. The interpretation of a neutral surface charge and its relevance in bioavailability and biocompatibility is ambiguous in currently available literature. In liposomes a neutral surface charge was shown to be desirable since negative and positive charged particles were eliminated more rapidly after IV administration in rats (32). Micro- and nanoemulsions containing non-ionic surfactants and co-surfactants have displayed excellent bioavailability and no toxicity when tested in animal models such as male Sprague Dawley rats (33) and Kunming mice (23). Nonionic NEs have also been tolerated well in cell cultures as well (34).

Differential Scanning Calorimetry

This experiment was performed to verify the absence of any un-dissolved CBZ in the SNE mixture. The DSC thermograms are shown in Fig. 4. Pure carbamazepine showed a sharp endothermic peak with an onset at 189°C and a peak temperature of 192°C. This data is consistent with that reported in the literature and is attributed to the melting of the α polymorph of CBZ (35). The enthalpy of fusion associated with this thermal event was found to be 105.43 J/g. The drug-loaded SNEDDS did not show thermal events that can be attributed to CBZ, indicating that CBZ was present in an

Table II Particle Size Analysis Data of Nanostructured Mists

Formulation	D_{10} (µm)	D_{50} (µm)	D_{90} (µm)	Respirable fraction (%)
Blank NE	3.03 ± 0.03	4.95 ± 0.07	9.54 ± 0.30	50.92 ± 1.34
CBZ NE	2.77 ± 0.01	4.22 ± 0.01	6.36 ± 0.02	69.10 ± 0.33

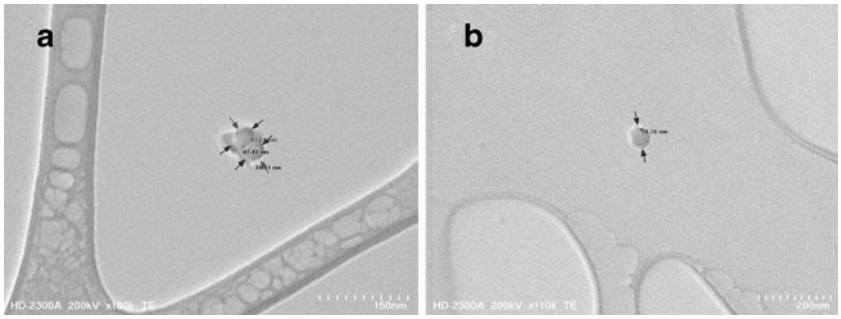

Fig. 7 TEM images of (**a**) blank nanoemulsion mist and (**b**) CBZ loaded nanoemulsion mist.

amorphous or molecular dispersion form (36). Solid crystalline material is characterized by a sharp endothermic transition during melting when subjected to a heating regimen in a DSC (35). Amorphous material and crystalline compounds that are present as a molecular dispersion do not exhibit sharp endothermic events when treated in the same manner. The absence of any peaks in the CBZ-SNE mixture conclusively indicated that the preparation did not contain CBZ in a solid particle form.

Transmission Electron Microscopy

Figure 5 represents the electron micrographs of nanoemulsion droplets when analyzed in the TEM. The size of droplets obtained using TEM was found to be larger than that determined by DLS. This phenomenon was repeatedly observed and could be attributed to the difference in experimental conditions used to prepare samples and perform TEM and DLS experiments. In DLS, liquid samples taken in a cuvette are placed in the path of a laser beam. The oil nanodroplets are capable of undergoing Brownian motion and hence undergo translational movement. The sample for TEM is essentially a drop of the O/W NE that is placed in a dimensionally constrained and flat TEM grid. As the water in the external phase evaporates after deposition, low surface tension facilitates spreading and the high surface-free energy of the nanodroplets leads to aggregation (37). Hence, the droplets assume a flat circular shape and appear larger in two dimensions. Similar data was noticed by other researchers when developing a nasal delivery system (38). We further detected this phenomenon when particle sizing standards of polystyrene latexes were visualized using TEM. It is remarkable that even in the presence of aggregation within the TEM grids, the size of the droplets was in the 100 nm range.

Size and Morphology of Nanostructured Mists

Figure 6 shows representative particle size distributions of the nanostructured mists, and Table II summarizes the data ($n=3$). The volume mean diameter D50 of the blank NE was found to be 4.95 ± 0.07 μm, and CBZ-loaded NE was found to be 4.23 ± 0.01 μm. The respirable fraction of blank NE was $50.92\pm0.92\%$ and that of CBZ NE was $69.10\pm0.33\%$. The respirable fraction represents the fraction of particles having a diameter less than 5 μm and capable of reaching the gas exchange areas within the lungs. The results suggest that the nanostructured mist reported in this work is suitable for pulmonary delivery of drugs and pharmaceuticals. The depth of penetration, site of deposition, and bioavailability of inhalation aerosols in the respiratory tract (RT) are dependent on the particle size (29). As particle size approaches and exceeds 5 μm, greater fractions of the inhaled material start depositing in the oropharyngeal region and upper RT. Formulations intended to deliver drugs into the lungs are hence manufactured with particles in the size range 1 to 5 μm (39). Although this is a generally accepted dogma, porous particles larger than 5 μm possessing appropriate aerodynamic properties were found to reach the lower RT as well (40).

The spreading and aggregation phenomenon observed in the aqueous NE droplets discussed in the previous section was seen in the TEM of mist droplets. Figure 7 presents the TEM image of the oil droplets deposited from the nanostructured mist collected on a TEM grid. The spreading of droplets on the TEM grid could be attributed to the surfactant and cosurfactant layer surrounding the oil droplet, as the

Table III Summary of Results of Sterility Validation Test Performed on MH Agar Plates Indicating the Presence (+) or Absence (−) of Microbial Growth

	Negative control	Positive control	Positive sample control	Sample
Day 0				
FTM	−	+	+	−
SCD 30 to 35°C	−	+	+	−
SCD 20 to 25°C	−	+	+	−
Day 7				
FTM	−	+	+	−
SCD 30 to 35°C	−	+	+	−
SCD 20 to 25°C.	−	+	+	−
Day 14				
FTM	−	+	+	−
SCD 30 to 35°C	−	+	+	−
SCD 20 to 25°C.	−	+	+	−

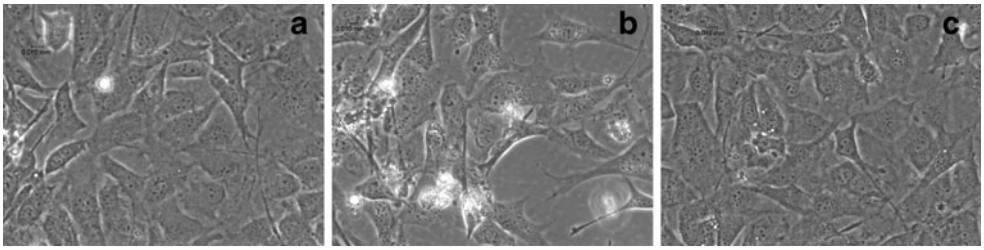

Fig. 8 Cells from *in vitro* cytoxicity assay observed under a light microscope (**a**) positive control (**b**) 11% sample concentration (**c**) 0.5% sample concentration.

surfactants are good spreading and wetting agents. Nonetheless, the integrity of the SNEDDS droplets and nebulization of the O/W NE were confirmed by the TEM experiment.

Validation of Sterilization Method

Nanoemulsion samples were analyzed using a direct inoculation and plate inoculation technique, utilizing two different broths according to USP guidelines. FTM was used for the growth and detection of anaerobic bacteria, while SCD was used for the detection of fungi and aerobes.

Formulations were filtered through 0.2 μm syringe filters under aseptic conditions. The filtered nanoemulsion was introduced into test tubes containing SCD and FTM and stored as described in the "Materials and Methods" section. All NE sample test tubes were visually inspected every day throughout the study period and did not show any phase separation. This was expected, since the NEs were O/W type and hence infinitely dilutable in aqueous media. All tubes from the direct inoculation method remained clear throughout the 14-day test period, except for the positive controls.

For plate inoculation, samples from test tubes were taken and transferred onto MH agar plates. Direct inoculation tubes were vortexed, and samples were withdrawn on days 0, 7, and 14 for plating. Plates were inspected for microbial growth after 24 h of incubation at 35°C (Table III). Only the positive controls showed growth on the plates and turbidity in the test tubes. Plates with the nanoemulsion did not show microbial growth throughout the 14-day test period. The results obtained from days 0, 7 and 14 successfully validated the aseptic sterilization method used for the nanoemulsion formulations. Similar results were obtained when we used identical methodology to develop and validate a sterilization method for water-in-oil microemulsions (41).

In Vitro Cytotoxicity Test

MTT calorimetric assay was used to examine the *in vitro toxicity* of the nanoemulsion in NIH 3T3 cells (mouse embryonic fibroblasts). The assay relies on the ability of viable cells to metabolize tetrazolium salt present in the MTT reagent to purple formazan product (42). Higher absorbance value is directly related to the amount of formazan present in a particular well, resulting in an intense purple color that indicates a higher number of viable cells. A one-way analysis of variance test (ANOVA) was conducted to examine the statistical significance of the MTT assay data at different concentrations of nanoemulsion after 48 h of exposure time. The *in vitro* cytotoxicity data are shown in Fig. 8 and Table IV. The cells tolerated nanoemulsion concentrations in the range of 0.125% to 5.5% v/v. Cells treated to 11% v/v NE demonstrated a statistically significant ($p<0.05$) difference in cell viability, indicating that this concentration was potentially not biocompatible. However, the decrease in the number of viable cells can also be produced due to dilution and deprivation of nutrients when 20% of liquid media from the wells was removed to produce an effective concentration of 11% NE in the wells. Concentration-dependent effects on cell viability have been observed when micro- and nanoemulsions containing similar components were tested *in vitro* in Caco-2 cultures (26), mouse embryonic fibroblasts NIH3T3 cells (43), and red blood cells (23). Published data connotes a tolerance that is related to the concentration used when cell cultures were exposed to these preparations. Similar formulations, when administered parenterally to beagle dogs (12) and Sprague Dawley rats (33), were found to be tolerated in the doses used in the studies. Several other animal models have received such formulations *via* various routes of delivery including topically in Syrian golden hamsters (30) and orally in Wistar rats (2), Sprague Dawley rats (27), and Kunming mice (23). In all these instances, the formulations were tolerated by the animals and found to offer biopharmaceutical advantages and enhance pharmacokinetic properties of model drugs.

In Vitro Permeability Studies in Zebra Fish Eggs

Before using Sudan IV-loaded NE in *in vitro* permeability studies, the physico-chemical properties of the dye-excipient

Table IV *In Vitro* Cytotoxicity of NE Obtained from MTT Assay ("−" Indicates No Toxicity, "+" Indicates Toxicity)

NE concentration % w/v	Toxicity
0.125	−
0.25	−
0.5	−
5.5	−
11	+

Table V Solubility of Sudan IV in Excipients

Excipient	Solubility (mg/ml)
Cremophor RH 40	38.433 ± 3.4
PEG 400	125.67 ± 11.2
Labrafil M 2125 CS	178 ± 6.9
DMSO	497 ± 9.4
Water	Practically insoluble

mixtures and dye-loaded NE were evaluated. The solubility of Sudan IV in individual excipients forming the nanoemulsion was determined using a UV–vis spectrophotometer. The dye showed good solubility in Labrafil M 2125 CS and practically no solubility in water. Table V summarizes the solubility of Sudan IV in various excipients. The pH of the Sudan IV-loaded NE containing 50 mg/mL dye was found to be 5.5 ± 0.3 and that of 100 mg/mL Sudan IV-loaded NE was 5.9 ± 0.2. Droplet size of the dye-loaded NE as determined by DLS was found to be 19 ± 2.1 nm and was not significantly different from the blank nanoemulsion. Similarly, the dye-loaded NE was found to be neutral when zeta potential analysis was performed. This demonstrated that the dye did not alter the electrical properties of the interface.

The *in vitro* permeability results obtained from zebra fish eggs exposed to various test preparations are shown in Fig. 9b. Figure 9a shows an egg exposed to egg water; Fig. 9b is an image showing an egg exposed to blank NE; Fig. 9c is an egg exposed to Sudan IV-loaded NE containing 50 mg/mL dye; and 9 (d) is an egg treated with 100 mg/mL Sudan IV-loaded NE. The negative and positive controls do not show any fluorescence. A concentration-dependent increase in the intensity of fluorescence is seen in Fig. 9c and d. The transparent outer covering of the egg is the acellular chorion, which plays a role in sperm-egg interaction, prevents polyspermy, and protects the developing embryo. The formulation has permeated through the chorion, which is a multilayered muchopolysaccharide envelope that contains glycoproteins as a predominant macromolecular component (44). The presence of fluorescence in the darker inner spherical region indicates that the formulation, after passing through the chorion, is starting to partition into the cells of the developing embryo.

In Vitro Permeability Studies in HeLa Cells

Figure 10 shows Z-stack images obtained from *in vitro* permeability studies performed in HeLa cell cultures. Figure 10a shows cells treated with culture medium, Fig. 10b shows cells treated with blank NE, and Fig. 10c shows cells treated with dye-NE containing 100 mg Sudan IV/mL of the nanoemulsion. The white crosshairs are through a healthy cell and indicate the axes along which the cell was scanned to determine the density of Sudan IV incorporated within the cell. The image strip on the right of each panel shows the data scanned along the horizontal axes (XZ) and the image strip below each panel indicates the data scanned along the vertical axes (YZ). In Fig. 10a no fluorescence is visible when tracing the path along the lines into the strips to the right and below the image. Minimal fluorescence is observed in cells that are particularly spherical in shape. This phenomenon is generally observed in cells that are undergoing apoptosis and that demonstrate a propensity of fluorescent biomacromolecules on the cell surface and intracellularly at this stage of life cycle (45). Figure 10b shows the data from cells exposed to blank NE. Similar to negative control some fluorescence is observed in spherical cells. However no fluorescence is seen in the healthy and elongated cells through which the scanning axes cross. Figure 10c represents cells treated to Sudan IV loaded NE in which the scan axes are positioned along a healthy cell. The cell in itself, and image strips to the right of the panel and below the image shows fluorescence uniformly around each scan axis. These results validate the localization of the dye in the interior of the cell.

In Vitro Permeability Studies in Porcine Lungs

Since the formulation was intended for pulmonary delivery, porcine lung tissue was used to investigate *in vitro* permeation of the fluorescent dye, Sudan IV. The porcine model is widely accepted and used to simulate human conditions in *in vitro* and *in vivo* experiments (46). Histological analysis was used to examine the diffusion of the fluorescent dye-loaded nanoemulsion through the porcine lung tissue. Cryotome

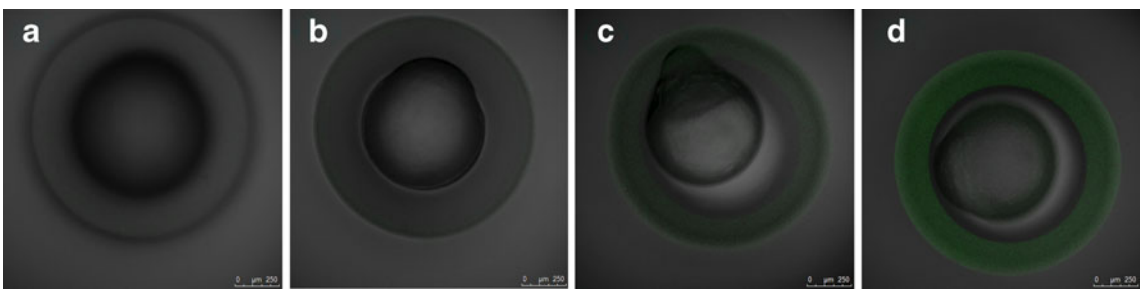

Fig. 9 CLSM images of *in vitro* permeability results obtained from zebra fish eggs (**a**) egg exposed to egg water (**b**) egg exposed to blank NE (**c**) egg exposed to Sudan IV loaded NE containing 50 mg/mL dye (**d**) egg treated with 100 mg/mL dye loaded NE.

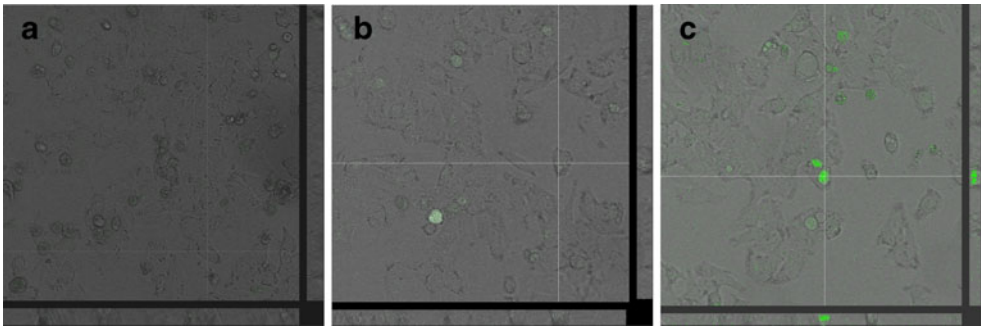

Fig. 10 CLSM images obtained from *in vitro* permeability studies performed in HeLa cell cultures (**a**) Cells treated with culture medium (**b**) Cells treated with blank NE (**c**) cells treated with dye-NE containing 100 mg Sudan IV/mL.

sections were visualized under a high-resolution fluorescence microscope to observe the disposition of dye inside the tissue. When sectioning the tissue samples, slices were made along the sagittal plane. This method was used so that when mounted on a slide and placed in the microscope, the images would present the tissue in a manner such that the upper part of the picture represents the region exposed to a particular test preparation and the lower part represents the area closer to the receptor chamber of the Franz diffusion cell. Thin cryosections of appropriately exposed porcine tissue were mounted on a glass slide and observed in order to examine the dye-labeled nanoemulsion. DAPI was used as a counterstain to stain the nucleolus of the cells (47). Since Sudan IV has a different excitation and emission wavelength than DAPI, it will exhibit a fluorescent green color, while DAPI will stain the nuclei blue, offering a good contrast when images captured at their respective wavelengths are overlaid. Figure 11 presents DAPI fluorescence, Sudan IV fluorescence, and the overlay images of fluorescences for negative control, positive control and dye-loaded NE tissues. Figure 11a–c are the images obtained from negative control tissue samples. In Fig. 11a, the nuclei are stained blue, suggesting that they took up the DAPI dye. Figure 11b does not show any fluorescence when scanned in the fluorescence wavelength corresponding to Sudan IV, indicating that the buffer did not possess any fluorescence in the wavelength scanned. Figure 11c, which is an overlay of (a) and (b), hence shows only the blue stain produced by DAPI. Similarly, analysis of Fig. 11d–f, which correspond to lung tissue exposed to blank NE, shows the DAPI-stained nuclei in blue, but the NE in itself does not fluoresce at the scanned wavelengths. Image shown in Fig. 11g–i correspond to the lung tissue exposed to Sudan IV-loaded NE. Figure 11g shows blue stained nuclei; Fig. 11h shows the green fluorescence of Sudan IV in the tissue; and Fig. 11i, which is an overlay of (g) and (h), enables differentiation of the nuclei and identification of the dye in the lung tissue. It may be noted that the upper part of the image is approximately the

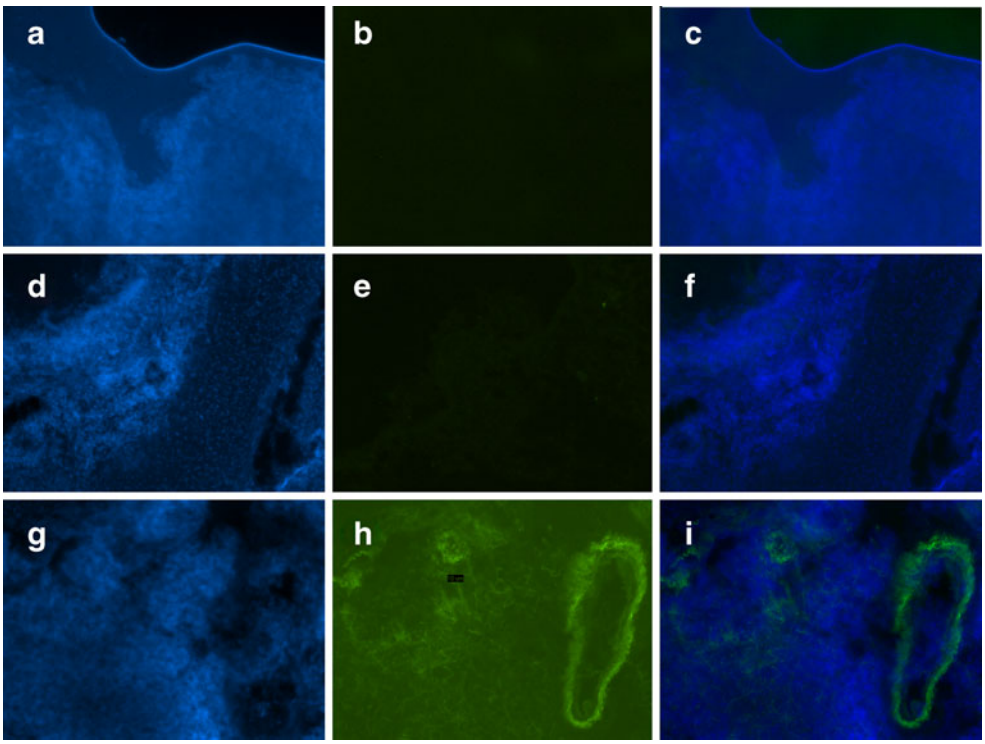

Fig. 11 Fluorescence microscopy images obtained from *in vitro* permeability studies performed in porcine lung tissue (**a**) tissue treated with buffer under DAPI filter (**b**) tissue treated with buffer under FITC filter (**c**) overlay of (**a**) and (**b**) (**d**) tissue treated with blank NE under DAPI filter (**e**) tissue treated with blank NE under FITC filter (**f**) overlay of (**d**) and (**e**) (**g**) tissue treated with Sudan IV loaded NE under DAPI filter (**h**) tissue treated with Sudan IV loaded NE under FITC filter (**i**) overlay of (**g**) and (**h**).

region where the tissue was exposed to the dye-loaded NE, and the lower region resided close to the receptor chamber. These results provide further undisputable evidence that the formulation permeates through the multiple cell layers in lung tissue, partitioning into various anatomical regions along with localization inside the porcine tissue.

CONCLUSION

In this study, a self-nanoemulsifying mixture was developed and investigated for its potential use in pulmonary drug delivery as a novel nanostructured mist. Various lipid excipients, surfactants, and co-surfactants were combined systematically to evaluate their self-nanoemulsifying properties. The combination consisting of 50% Cremophor RH 40, 25% PEG 400 and 25% Labrafil M 2125 CS was selected as the optimal formulation for drug incorporation. Carbamazepine was selected as a model drug for incorporation into the nanoemulsion to assess the system's suitability to carry poorly water-soluble compounds. The developed nanoemulsions possessed a diameter less than 20 nm and a neutral zeta potential. Solubility studies and DSC experiments confirmed that CBZ was present in a molecularly dispersed state in the formulation. TEM studies of aqueous nanoemulsions and nanostrucutured mists delineated the structure and morphology of the formulation. Data from laser diffraction studies confirmed the droplet size of the nebulized mist and affirmed its suitability for pulmonary delivery. The aseptic sterilization method developed and validated in this work is amenable to scale-up. The formulation was tolerated in NIH3T3 cells, indicating its biocompatibility. *In vitro* permeability tests performed in zebra fish eggs, HeLa cells, and porcine lung tissue support good permeability for the formulation and its ability to internalize within cell and biological structures. The results substantiate the capability of the reported formulation to be developed into a viable pulmonary delivery system. Ongoing work includes utilization of drug-loaded NE to evaluate biodistribution and absorption of a novel analogue to treat alcohol dependence when tested in alcohol-preferring P-rats.

ACKNOWLEDGMENTS AND DISCLOSURES

This research was performed with support from start-up funds made available by the Department of Pharmacy Practice at the University of Toledo College of Pharmacy and Pharmaceutical Sciences. We are grateful to Dr. Joseph Lawrence, Center for Sensor and Materials Characterization, University of Toledo College of Engineering for his assistance during the TEM work. We also thank Ms. Maki Takahashi, Department of Pharmacology, University of Toledo College of Pharmacy and Pharmaceutical Sciences for her help with cell cultures.

REFERENCES

1. Nazzal S, Smalyukh II, Lavrentovich OD, Khan MA. Preparation and in vitro characterization of a eutectic based semisolid self-nanoemulsified drug delivery system (SNEDDS) of ubiquinone: mechanism and progress of emulsion formation. Int J Pharm. 2002;235(1–2):247–65.
2. Shafiq S, Shakeel F, Talegaonkar S, Ahmad FJ, Khar RK, Ali M. Development and bioavailability assessment of ramipril nanoemulsion formulation. Eur J Pharm Biopharm. 2007;66(2):227–43.
3. Wang L, Dong J, Chen J, Eastoe J, Li X. Design and optimization of a new self-nanoemulsifying drug delivery system. J Colloid Interface Sci. 2009;330(2):443–8.
4. Lawrence MJ, Rees GD. Microemulsion-based media as novel drug delivery systems. Adv Drug Deliv Rev. 2000;45(1):89–121.
5. Kawakami K, Yoshikawa T, Hayashi T, Nishihara Y, Masuda K. Microemulsion formulation for enhanced absorption of poorly soluble drugs: II. In vivo study. J Control Release. 2002;81(1–2):75–82.
6. Lipinski CA, Lombardo F, Dominy BW, Feeney PJ. Experimental and computational approaches to estimate solubility and permeability in drug discovery and development settings. Adv Drug Deliv Rev. 2001;46(1–3):3–26.
7. Stevens RE, Limsakun T, Evans G, Mason Jr DH. Controlled, multidose, pharmacokinetic evaluation of two extended-release carbamazepine formulations (Carbatrol and Tegretol-XR). J Pharm Sci. 1998;87(12):1531–4.
8. El-Zein H, Riad L, El-Bary AA. Enhancement of carbamazepine dissolution: in vitro and in vivo evaluation. Int J Pharm. 1998;168(2):209–20.
9. Custodio JM, Wu CY, Benet LZ. Predicting drug disposition, absorption/elimination/transporter interplay and the role of food on drug absorption. Adv Drug Deliv Rev. 2008;60(6):717–33.
10. Patton JS, Byron PR. Inhaling medicines: delivering drugs to the body through the lungs. Nat Rev Drug Discov. 2007;6(1):67–74.
11. Hoover JL, Rush BD, Wilkinson KF, Day JS, Burton PS, Vidmar TJ, *et al.* Peptides are better absorbed from the lung than the gut in the rat. Pharm Res. 1992;9(8):1103–6.
12. Kang BK, Lee JS, Chon SK, Jeong SY, Yuk SH, Khang G, *et al.* Development of self-microemulsifying drug delivery systems (SMEDDS) for oral bioavailability enhancement of simvastatin in beagle dogs. Int J Pharm. 2004;274(1–2):65–73.
13. Craig DQM, Lievens HSR, Pitt KG, Storey DE. An investigation into the physico-chemical properties of self-emulsifying systems using low frequency dielectric spectroscopy, surface tension measurements and particle size analysis. Int J Pharm. 1993;96(1–3):147–55.
14. United States Pharmacopeial Convention. The United States pharmacopeia: the national formulary. Rockville: United States Pharmacopeial Convention; 2006.
15. Nesamony J, Zachar CL, Jung R, Williams FE, Nauli S. Preparation, characterization, sterility validation, and in vitro cell toxicity studies of microemulsions possessing potential parenteral applications. Drug Dev Ind Pharm. 2012;5:5.
16. Kumar S, Singh HN. Competitive solubilization of Sudan IV and anthracene in micellar systems. Colloids Surf. 1992;69(1):1–4.
17. Krishna SM, Seto SW, Moxon JV, Rush C, Walker PJ, Norman PE, *et al.* Fenofibrate increases high-density lipoprotein and sphingosine 1 phosphate concentrations limiting abdominal aortic aneurysm progression in a mouse model. Am J Pathol. 2012;181(2):706–18.
18. Rebane R, Leito I, Yurchenko S, Herodes K. A review of analytical techniques for determination of Sudan I-IV dyes in food matrixes. J Chromatogr A. 2010;1217(17):2747–57.
19. Behrens I, Pena AIV, Alonso MJ, Kissel T. Comparative uptake studies of bioadhesive and non-bioadhesive nanoparticles in human intestinal cell lines and rats: the effect of mucus on particle adsorption and transport. Pharm Res. 2002;19(8):1185–93.

20. Hahnenkamp I, Graubner G, Gmehling J. Measurement and prediction of solubilities of active pharmaceutical ingredients. Int J Pharm. 2010;388(1–2):73–81.
21. Abid SK, Hamid SM, Sherrington DC. Micellization and surface-activity of long-chain monoquaternary and diquaternary ammonium salts. J Colloid Interface Sci. 1987;120(1):245–55.
22. Kibbe AH. Handbook of pharmaceutical excipients. Washington, DC: American Pharmaceutical Association; 2000.
23. Li G, Fan Y, Li X, Wang X, Li Y, Liu Y, *et al.* In vitro and in vivo evaluation of a simple microemulsion formulation for propofol. Int J Pharm. 2012;425(1–2):53–61.
24. Shinoda K, Shibata Y, Lindman B. Interfacial tensions for lecithin microemulsions including the effect of surfactant and polymer addition. Langmuir. 1993;9(5):1254–7.
25. Kahlweit M, Strey R, Schomaecker R, Haase D. General patterns of the phase behavior of mixtures of water, nonpolar solvents, amphiphiles, and electrolytes. 2. Langmuir. 1989;5(2):305–15.
26. Sha X, Yan G, Wu Y, Li J, Fang X. Effect of self-microemulsifying drug delivery systems containing Labrasol on tight junctions in Caco-2 cells. Eur J Pharm Sci. 2005;24(5):477–86.
27. Kawakami K, Yoshikawa T, Moroto Y, Kanaoka E, Takahashi K, Nishihara Y, *et al.* Microemulsion formulation for enhanced absorption of poorly soluble drugs I. Prescription design. J Control Release. 2002;81(1–2):65–74.
28. Gershanik T, Benzeno S, Benita S. Interaction of a self-emulsifying lipid drug delivery system with the everted rat intestinal mucosa as a function of droplet size and surface charge. Pharm Res. 1998;15(6):863–9.
29. Adjei A, Garren J. Pulmonary delivery of peptide drugs: effect of particle size on bioavailability of leuprolide acetate in healthy male volunteers. Pharm Res. 1990;7(6):565–9.
30. Kotyla T, Kuo F, Moolchandani V, Wilson T, Nicolosi R. Increased bioavailability of a transdermal application of a nano-sized emulsion preparation. Int J Pharm. 2008;347(1–2):144–8.
31. Kommuru TR, Gurley B, Khan MA, Reddy IK. Self-emulsifying drug delivery systems (SEDDS) of coenzyme Q10: formulation development and bioavailability assessment. Int J Pharm. 2001;212(2):233–46.
32. Gabizon A, Papahadjopoulos D. The role of surface charge and hydrophilic groups on liposome clearance in vivo. Biochim Biophys Acta. 1992;10(1):94–100.
33. Park K-M, Kim C-K. Preparation and evaluation of flurbiprofen-loaded microemulsion for parenteral delivery. Int J Pharm. 1999;181(2):173–9.
34. Kotmakchiev M, Kantarci G, Cetintas VB, Ertan G. Cytotoxicity of a novel oil/water microemulsion system loaded with mitomycin-C in in vitro lung cancer models. Drug Dev Res. 2012;73(4):185–95.
35. Katzhendler I, Azoury R, Friedman M. The effect of egg albumin on the crystalline properties of carbamazepine in sustained release hydrophilic matrix tablets and in aqueous solutions. J Control Release. 2000;65(3):331–43.
36. Vasconcelos T, Sarmento B, Costa P. Solid dispersions as strategy to improve oral bioavailability of poor water soluble drugs. Drug Discov Today. 2007;12(23–24):1068–75.
37. Zhang D, Hamilton PD, Kao JLF, Venkataraman S, Wooley KL, Ravi N. Formation of nanogel aggregates by an amphiphilic cholesteryl-poly(amidoamine) dendrimer in aqueous media. J Polymer Sci, Part A: Polymer Chem. 2007;45(12):2569–75.
38. Sintov AC, Levy HV, Botner S. Systemic delivery of insulin *via* the nasal route using a new microemulsion system: In vitro and in vivo studies. J Control Release. 2010;148(2):168–76.
39. Elversson J, Millqvist-Fureby A, Alderborn G, Elofsson U. Droplet and particle size relationship and shell thickness of inhalable lactose particles during spray drying. J Pharm Sci. 2003;92(4):900–10.
40. Edwards DA, Hanes J, Caponetti G, Hrkach J, Ben-Jebria A, Eskew ML, *et al.* Large porous particles for pulmonary drug delivery. Science. 1997;276(5320):1868–71.
41. Nesamony J, Zachar CL, Jung R, Williams FE, Nauli S. Preparation, characterization, sterility validation, and in vitro cell toxicity studies of microemulsions possessing potential parenteral applications. Drug Dev Ind Pharm. 2013;39(2):240–51.
42. Twentyman PR, Luscombe M. A study of some variables in a tetrazolium dye (MTT) based assay for cell growth and chemosensitivity. Br J Cancer. 1987;56(3):279–85.
43. Lo J-T, Chen B-H, Lee T-M, Han J, Li J-L. Self-emulsifying O/W formulations of paclitaxel prepared from mixed nonionic surfactants. J Pharm Sci. 2010;99(5):2320–32.
44. Bonsignorio D, Perego L, Del Giacco L, Cotelli F. Structure and macromolecular composition of the zebrafish egg chorion. Zygote. 1996;4(2):101–8.
45. Levitt JM, Baldwin A, Papadakis A, Puri S, Xylas J, Munger K, *et al.* Intrinsic fluorescence and redox changes associated with apoptosis of primary human epithelial cells. J Biomed Opt. 2006;11(6):064012/1–/10.
46. Rothkotter H-J. Anatomical particularities of the porcine immune system–a physician's view. Dev Comp Immunol. 2009;33(3):267–72.
47. Williamson DH, Fennell DJ. The use of fluorescent DNA-binding agent for detecting and separating yeast mitochondrial DNA. Methods Cell Biol. 1975;12:335–51.